JOURNAL OF SPACECRAFT AND ROCKETS
Vol. 59, No. 1, January–February 2022

Diamagnetically Enhanced Electrolysis and Phase Separation in Low Gravity

Álvaro Romero-Calvo* and Hanspeter Schaub†
University of Colorado Boulder, Boulder, Colorado 80303
and
Gabriel Cano-Gómez‡
University of Seville, Sevilla, Spain 41092

https://doi.org/10.2514/1.A35021

The management of fluids in space is complicated by the absence of relevant buoyancy forces. This raises significant technical issues for two-phase flow applications. Different approaches have been proposed and tested to induce phase separation in low gravity; however, further efforts are still required to develop efficient, reliable, and safe devices. The employment of diamagnetic buoyancy is proposed as a complement or substitution of current methods and as a way to induce the early detachment of gas bubbles from their nucleation surfaces. The governing magnetohydrodynamic equations describing two-phase flows in low gravity are presented with a focus on bubble dynamics. Numerical simulations are employed to demonstrate the reachability of current magnets under different configurations, compare diamagnetic and Lorentz forces on alkaline electrolytes, and suggest scaling up procedures. The results support the employment of new-generation centimeter-scale neodymium magnets for electrolysis, boiling, and phase separation technologies in space, which would benefit from reduced complexity, mass, and power requirements.

Nomenclature

A	=	effective surface of the electrode, m^2
$\boldsymbol{B}$	=	magnetic flux density, T
$\boldsymbol{D}$	=	electric displacement field, C/m^2
D_0	=	contact line diameter, m
d_b	=	electrolytic bubble break-off diameter, m
d_0	=	bubble break-off diameter, m
$\boldsymbol{E}$	=	electric field, V/m
$\boldsymbol{e}_i$	=	Cartesian frame
$\boldsymbol{F}$	=	force, N
$\boldsymbol{f}^S$	=	surface force density, N/m^2
$\boldsymbol{f}^V$	=	body force density, N/m^3
$\boldsymbol{g}$	=	inertial acceleration, m/s^2
$\boldsymbol{H}$	=	magnetic field, A/m
$\boldsymbol{H}_0$	=	applied magnetic field, A/m
$\boldsymbol{H}^*$	=	virtual magnetic field, A/m
$\mathcal{H}$	=	arithmetic mean interface curvature, 1/m
$\boldsymbol{I}$	=	identity matrix
I	=	electrode current intensity, A
$\boldsymbol{J}_e$	=	electric current density, A/m^2
$\boldsymbol{K}_s$	=	surface electric current density, A/m
$\boldsymbol{k}$	=	normal vector perpendicular to the bubble pit
$\mathcal{L}$	=	Lorentz force per unit volume, N/m^3
$\boldsymbol{M}$	=	magnetization field, A/m
$\mathcal{M}$	=	molar mass, kg/mol
$m_b{}'$	=	virtual bubble mass, kg
$\boldsymbol{n}$	=	external normal vector
$\boldsymbol{P}$	=	electric polarization field, C/m^2
p	=	hydrostatic pressure, Pa
p_i	=	mass fraction
p^*	=	composite pressure, Pa
R_b	=	bubble radius, m
Re	=	Reynolds number
T	=	temperature, K
T	=	Maxwell stress tensor, Pa
$\boldsymbol{t}$	=	stress vector, Pa
$\boldsymbol{t}_{\mathrm{fg}}$	=	tangent unit vector in the meridian plane
ν	=	specific volume, m^3/kg
$\boldsymbol{v}$	=	fluid velocity, m/s
$\boldsymbol{v}_t$	=	terminal velocity, m/s
$\boldsymbol{x}$	=	position vector, m
γ	=	volume coefficient of viscosity, Pa · s
$\Delta\chi^{\mathrm{vol}}$	=	differential volume magnetic susceptibility
ϵ_0	=	permittivity of free space, F/m
η	=	dynamic coefficient of viscosity, Pa · s
θ	=	apparent contact angle, rad
λ	=	combined coefficient of viscosity, Pa · s
μ_0	=	permeability of free space, H/m
ρ	=	fluid density, kg/m^3
ρ_v	=	free charge density, C/m^3
σ	=	surface tension, N/m
σ_s	=	surface free charge density, C/m^2
χ^{mass}	=	mass magnetic susceptibility, m^3/kg
χ^{mol}	=	mole magnetic susceptibility, m^3/mol
χ^{vol}	=	volume magnetic susceptibility

Subscripts

e	=	electric term
f	=	liquid environment
g	=	gas environment
in	=	inertial
m	=	magnetic term
me	=	magnetic environment
n	=	normal component
p	=	pressure term
t	=	tangential component
ν	=	viscous term
σ	=	surface tension term

Received 14 November 2020; revision received 11 April 2021; accepted for publication 18 May 2021; published online 23 July 2021.

*Graduate Research Assistant, Department of Aerospace Engineering Sciences; alvaro.romerocalvo@colorado.edu. Student Member AIAA.

†Professor, Glenn L. Murphy Chair in Engineering, Department of Aerospace Engineering Sciences; hanspeter.schaub@colorado.edu. Member AIAA.

‡Associate Professor, Departamento de Física Aplicada III; gabriel@us.es.

I. Introduction

THE term *water electrolysis* refers to the electrochemical decomposition of water into hydrogen and oxygen. The reaction was

first performed by Troostwijk and Deiman in 1789 [1,2] and was already considered for space applications in the early 1960s [3]. A wide range of environmental control and life support systems [4], space propulsion technologies [5–7], and energy conversion and storage mechanisms [8,9] rely on this process. Furthermore, future interplanetary missions are likely to employ water as a commodity acquired and processed by in situ resource utilization (ISRU) methodologies to produce propellants, thereby reducing vehicle launch mass [10,11].

Water electrolysis technologies can be classified according to the nature of the electrolyte. Three chemistries are considered for space applications: alkaline, proton exchange membrane (PEM), and solid oxide ceramics. Of these, the low-temperature alkaline and PEM electrolytes require phase separation at the electrode. The liquid alkaline technology employs two metallic electrodes separated by a porous material and immersed in a conductive aqueous solution, usually prepared with KOH or NaOH. The cell separator allows the exchange of the OH^- groups and prevents the recombination of H_2 and O_2 into water. PEM cells, on the contrary, are fed with pure water and make use of a proton-conducting polymer electrolyte. PEM cells allow high current densities, prevent the recombination of oxygen and hydrogen (and so they are safer), and produce high-purity gases. However, they lack the long-term heritage of alkaline cells and are sensitive to water impurities [12].

The operation of alkaline and PEM cells in low gravity is severely complicated by the absence of strong buoyancy forces, resulting in increased complexity, mass, and power consumption. Dedicated microgravity experiments have shown how the weak buoyancy force gives rise to a layer of gas bubbles over the electrodes, shielding the active surface and limiting mass transport [13–15]. Gas bubbles tend to be larger than in normal-gravity conditions due to the longer residence time on the electrodes and the absence of bubble departure. Besides, and unlike in normal gravity, the bubble departure diameter increases with increasing current intensity [16]. A forced water flow can be employed to flush this structure, but this approach increases the complexity of the system and has a limited efficiency [17]. Most types of electrolytic cells also require a liquid/gas phase separation stage. Rotary [18,19] and membrane-type [17,20] devices are nowadays employed. Passive approaches that make use of surface tension by means wedge geometries [21,22], springs [23], or eccentric annuli [24] have also been proposed and tested. As an alternative, the generation of an equivalent dielectric buoyancy force by means of strong electric fields has been considered since the early 1960s [25] and has been studied and successfully tested for low-gravity boiling [26,27] and two-phase flow [28,29] applications. However, the drawbacks of these approaches are numerous: centrifuges add to system power loads and may represent a safety hazard, membranes have limited lifetime and tend to clog in the presence of water impurities [5,30], surface-tension-based approaches require careful geometrical design and are sensitive to moderate departures from the operational design point [21], and electric fields consume power and may represent a safety hazard for both human and autonomous spaceflight due to the large required potential differences.

Both alkaline and PEM technologies have flown to space and dealt with the phase separation problem in different ways. The Russian Elektron module, first operated at Mir and then at the International Space Station (ISS), makes use of a circulating alkaline electrolyte (25%wt KOH) and a fluid circuit with gas/liquid static separators and heat exchangers [31]. The operation of the system has been compromised in the past by notorious malfunction events [32–34]. NASA's Oxygen Generation System (OGS), installed at the ISS in July 2006, makes use of a cathode-feed PEM and a rotary phase separator and absorber modules to produce dry oxygen. Unlike anode-feed PEMs, cathode feeding avoids the humidification of O_2 due to proton-induced electro-osmosis [5]. Technical problems associated with the management of two-phase flows in the OGS in microgravity have also been reported [18,35]. The Japan Aerospace Exploration Agency (JAXA) has recently developed a cathode-feed PEM cell for O_2 generation. The system relies on the removal of the electrode gas cover by means of forced convection. The separation of gas hydrogen and liquid water is performed by means of a membrane-type phase separator [17,20,36]. Subsequent versions of the cathode-feed cell rely on an internal water/gas separation function that makes water circulation and phase separator unnecessary, creating a simple, energy-efficient, and lightweight system. However, difficulties were found to reach a stable phase separation process [37–39]. As a way to remove the water purification and phase separation stages, substantial efforts have been devoted to the development of static water feed (SWF) electrolytic cells, which avoid the phase separation stage by means of a second PEM. Technological demonstrators by Life Systems were tested on the STS-69 Endeavor (1995) and the STS-84 Atlantis (1997) for NASA [40–45], being followed by relatively modern systems [5,46]. In spite of its inherent advantages, this approach requires larger cells to deliver a specific gas output due to the presence of a second membrane, which increases the water gradient, and the adoption of a cathode-feed configuration for the second membrane [5,36].

This scientific and technological review unveils the numerous challenges associated with the low-gravity gas/liquid separation process and shows important limitations in current and foreseen technologies. As a complement or substitution of the previous methods, the inherent magnetic properties of water and water-based electrolytes may be employed to induce the natural detachment and collection of gas bubbles. Inhomogeneous magnetic fields induce a weak body force in continuous media [47] that, due to the differential magnetic properties between phases, results in a net buoyancy force. This phenomenon is known as magnetic buoyancy and has been applied to terrestrial boiling experiments with ferrofluids [48,49]. Previous works on low-gravity magnetohydrodynamics have explored the diamagnetic manipulation of air bubbles in water [50,51], the positioning of diamagnetic materials [52], air–water separation [53], protein crystal growth [54], magnetic positive positioning [55–59], magnetic liquid sloshing [60,61], or combustion enhancement [51], among others. The application of Lorentz's force on liquid electrolytes has also been studied as a way to enhance hydrogen production [62–72]. However, the use of magnetic buoyancy in phase separation, electrolysis, and boiling in low gravity remains largely unexplored.

The development of low-gravity magnetic phase separators may lead to reliable, lightweight, and passive devices. If the magnetic force was applied directly over the electrodes, the bubble departure diameter would be reduced and a convective flow would be induced on the layer of bubbles, enlarging the effective electrode surface and minimizing the mass transport limitations and cell voltage. The same benefits would be obtained for low-gravity boiling devices, with the boiling surfaces being equivalent to the electrodes.

In this paper, the applications of magnetic buoyancy in low-gravity electrolysis are first explored in Sec. II. A set of general theoretical tools that enable a comprehensive analysis of the problem are derived in Sec. III, whereas an analysis of bubble dynamics is given in Sec. IV. Fundamental results and technical solutions are shown in Sec. V, and conclusions are finally drawn in Sec. VI.

II. Magnetic Buoyancy Applications to Low-Gravity Water Electrolysis

The application of magnetic buoyancy may be beneficial for at least two common components of low-gravity water electrolysis systems: the electrolytic cell and the gas/liquid phase separator. These elements are present in both alkaline and PEM cells, with the exception of SFW configurations. As shown in Sec. III.D, magnetic buoyancy can be induced in virtually all liquids of technical interest, with pure water being the least magnetically susceptible of them. Although this discussion focuses on water electrolysis, the concepts here introduced have a direct equivalent in applications involving pool boiling or bubble growth, such as water boiling or other types of electrolysis, recombination, or combustion reactions.

A. Electrolytic Cells

The application of strong inhomogeneous magnetic fields over the electrodes would potentially induce a convective flow on the layer of bubbles, reducing the break-off diameter, enlarging the effective

surface, and reducing the cell voltage while effectively separating the phases. Some of these effects have been observed in terrestrial boiling experiments with ferrofluids, where a significant influence of the magnetic field on the boiling plate bubble coverage and heat transfer coefficient is reported [48,49].

Depending on the type of reactant, the diamagnetic or para/ferromagnetic configurations depicted in Fig. 1 should be considered. Whereas in the former a diamagnetic liquid (such as water) is repelled from the magnet, in the latter a paramagnetic or ferromagnetic substance is employed, producing the opposite effect. In virtue of Archimedes's principle, gas bubbles experience a magnetic buoyancy force that attracts (diamagnetic) or expels (para/ferromagnetic) them from the magnet.

This distinction may sound contrived to the reader, as water and its associated electrolytes are diamagnetic materials and applications where paramagnetic or ferromagnetic substances are employed cannot be easily found. However, the renewed interest in nanofluids-enhanced [73] and magnetically enhanced [48,49] heat transfer may open new interesting avenues of research. Highly susceptible liquids, such as ferrofluids, may be employed to boost the productivity of the electrodes and boiling surfaces, both on Earth and in space. In spite of the numerous technical challenges that such technologies would face (e.g., thermal stability or particle deposition [74]), the possibility of using ferrofluids is covered by this work.

B. Phase Separators

Although the magnetic electrolytic cell concept presents intrinsic advantages, modularity is commonly sought in an industry characterized by a complicated and expensive design flow. From a systems engineering perspective, magnetic phase separators could replace the functionality of existing phase separation technologies without forcing qualitative modifications at the cell level, and with applications to any combination of phases. The magnetic buoyancy force could also be employed in combination with existing systems, such as surface-tension-enabled phase separators.

This is conceptually represented in Fig. 2, where magnetic and combined surface tension/magnetic phase separators are shown for a dielectric liquid. The magnetic phase separator consists on a channel surrounding a magnet that attracts the bubbles from an incoming two-phase flow. The combined phase separator consists on a wedge-shaped channel that pushes large bubbles to the open end as they evolve toward their configuration of minimum energy (spherical geometry). This approach was tested in the Capillary Channel Flow experiment, conducted at the ISS in April 2010 [21]. Magnetic

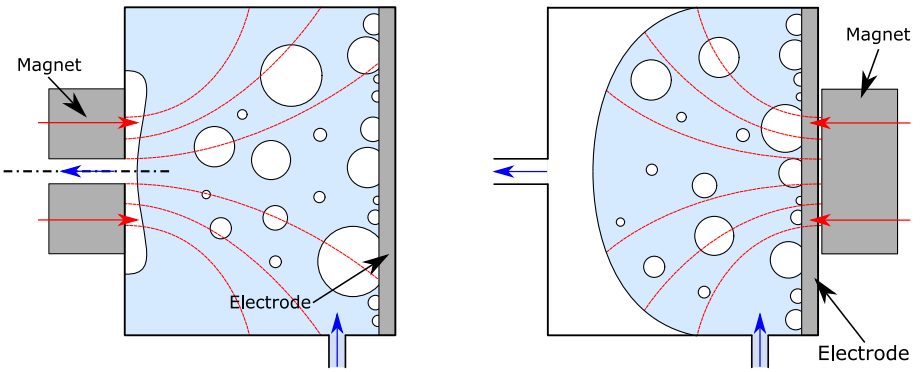

a) Diamagnetic b) Para/ferromagnetic

Fig. 1 Conceptual representation of a magnetically enhanced electrolysis cell. Blue arrows represent the liquid/gas flow, whereas red arrows denote the magnetization vector.

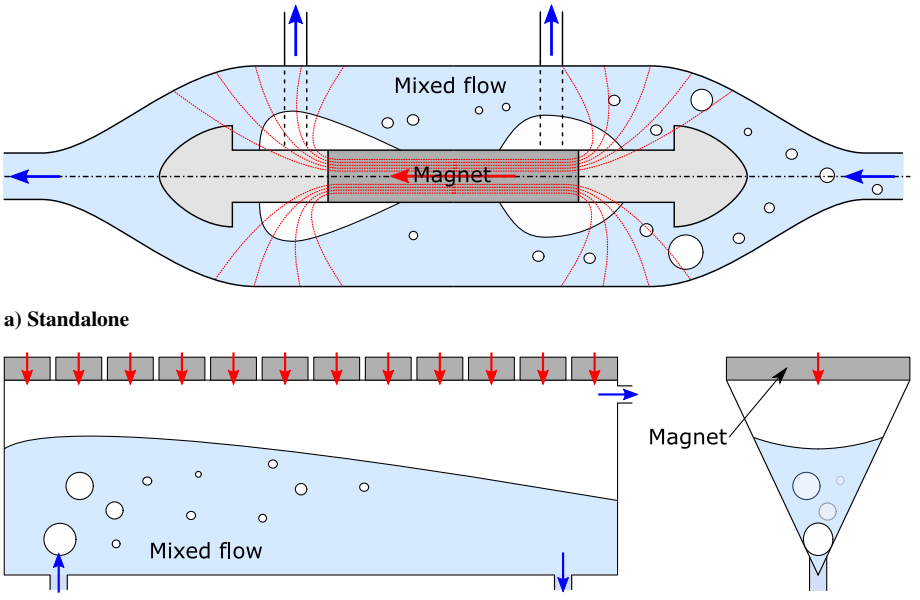

a) Standalone

b) Combined

Fig. 2 Conceptual representation of a magnetic standalone and surface-tension-enhanced diamagnetic phase separator. Blue arrows represent the liquid/gas flow, whereas red arrows denote the magnetization vector.

buoyancy may be particularly useful to attract small bubbles that are unlikely to contact the free surface and hence remain within the liquid flow.

III. Magnetic Buoyancy in Two-Phase Flows

The conceptual solutions here presented should be studied in the framework of the magnetohydrodynamic theory. This section introduces a series of fundamental theoretical tools together with simplified expressions that enable preliminary analyses. Because of their potential interest in future applications, the use of ferrofluids is considered. No assumptions are made regarding the constitutive relation of the material.

A. Governing Equations for Polarizable, Viscous, Compressible Fluids

The magneto/electrohydrodynamic mass and momentum conservation equations are given by [75]

$$\frac{\partial \rho}{\partial t} + \nabla \cdot (\rho \boldsymbol{v}) = 0 \tag{1a}$$

$$\rho \frac{D\boldsymbol{v}}{Dt} = \rho \boldsymbol{g} + \nabla \cdot \mathrm{T} \tag{1b}$$

subject to appropriate boundary conditions, with $\boldsymbol{v}$ being the velocity field, ρ the fluid density, $\boldsymbol{g}$ the inertial acceleration, D/Dt the material derivative, and T the Maxwell stress tensor that includes pressure, viscous, magnetic, and electric terms.

The stress tensor T is defined in terms of the magnetic and electric fields acting on the system. Those are computed from Maxwell equations:

$$\nabla \cdot \boldsymbol{D} = \rho_v \tag{2a}$$

$$\nabla \cdot \boldsymbol{B} = 0 \tag{2b}$$

$$\nabla \times \boldsymbol{E} = -\frac{\partial \boldsymbol{B}}{\partial t} \tag{2c}$$

$$\nabla \times \boldsymbol{H} = \boldsymbol{J}_e + \frac{\partial \boldsymbol{D}}{\partial t} \tag{2d}$$

where $\boldsymbol{E}$, $\boldsymbol{D} = \varepsilon_0 \boldsymbol{E} + \boldsymbol{P}$, and $\boldsymbol{P}$ are the electric, electric displacement, and polarization fields, and $\boldsymbol{B}$, $\boldsymbol{H} = (\boldsymbol{B}/\mu_0) - \boldsymbol{M}$, and $\boldsymbol{M}$ are the flux density, magnetic, and magnetization fields, respectively; ϵ_0 and μ_0 are the permittivity and permeability of vacuum, ρ_v is the free charge density, and $\boldsymbol{J}_e$ is the electric current density. For soft magnetic materials, the magnetization field is aligned with the magnetic field and follows the relation $\boldsymbol{M} = \chi^{\mathrm{vol}}(H)\boldsymbol{H}$, with $\chi^{\mathrm{vol}}(H)$ being the volume magnetic susceptibility. Dia/paramagnetic materials exhibit a constant and small χ^{vol}. The interfacial electric and magnetic boundary conditions are

$$\boldsymbol{n} \cdot (\boldsymbol{D}_2 - \boldsymbol{D}_1) = \sigma_s \tag{3a}$$

$$\boldsymbol{n} \times (\boldsymbol{E}_2 - \boldsymbol{E}_1) = 0 \tag{3b}$$

$$\boldsymbol{n} \cdot (\boldsymbol{B}_2 - \boldsymbol{B}_1) = 0 \tag{3c}$$

$$\boldsymbol{n} \times (\boldsymbol{H}_2 - \boldsymbol{H}_1) = \boldsymbol{K}_s \tag{3d}$$

with σ_s and $\boldsymbol{K}_s$ being the surface free charge and electric current densities, respectively. Therefore, the normal component of $\boldsymbol{B}$ and, in the absence of surface currents, the tangential component of $\boldsymbol{H}$, are continuous across the interface.

For most applications covered in this work, the dielectric force can be neglected (see the comparison between diamagnetic and dielectric terms in Sec. V.A) and the stationary Maxwell equations in the absence of electric charges are employed due to the consideration of a neutrally charged medium. The theoretical framework can be further simplified when considering dia/paramagnetic materials, whose small magnetization field justifies the approximation $\boldsymbol{H} \approx \boldsymbol{H}_0$, with $\boldsymbol{H}_0$ being the *applied* magnetic field. From a practical perspective, this implies that $\boldsymbol{H}_0$ can be calculated independently of the state of the system under analysis. A simplified set of governing equations for incompressible, neutral fluids subject to static magnetic fields is given in the Appendix.

B. Viscous Maxwell Stress Tensor

The magneto/electrodynamic state of a continuous medium can be described by means of the viscous Maxwell stress tensor, which has been formulated in the classical literature as [47,75–77]

$$\mathrm{T} = \mathrm{T}_p + \mathrm{T}_\nu + \mathrm{T}_m + \mathrm{T}_e \tag{4}$$

with the pressure, viscous, magnetic, and electric terms being given by

$$\mathrm{T}_p = -p^* \boldsymbol{I} \tag{5a}$$

$$\mathrm{T}_\nu = \eta[\nabla \boldsymbol{v} + (\nabla \boldsymbol{v})^T] + \lambda(\nabla \cdot \boldsymbol{v})\boldsymbol{I} \tag{5b}$$

$$\mathrm{T}_m = -\frac{\mu_0}{2} H^2 \boldsymbol{I} + \boldsymbol{B}\boldsymbol{H} \tag{5c}$$

$$\mathrm{T}_e = -\frac{\varepsilon_0}{2} E^2 \boldsymbol{I} + \boldsymbol{D}\boldsymbol{E} \tag{5d}$$

and where

$$p^* = p(\nu, T) + \mu_0 \int_0^H \frac{\partial}{\partial \nu}[\nu M]\mathrm{d}H' + \int_0^E \frac{\partial}{\partial \nu}[\nu P]\mathrm{d}E' \tag{6}$$

is the composite pressure, which includes hydrostatic $p(\nu, T)$ and magneto/electropolarization terms. In the previous expressions, $\boldsymbol{I} = \delta_{ij}\boldsymbol{e}_i\boldsymbol{e}_j$ is the unit dyadic in the Cartesian $\boldsymbol{e}_i$ reference system, and $\nu = \rho^{-1}$ is the specific volume of the medium. In the viscous tensor, $\lambda = (\gamma - 2\eta)/3$, and η and γ are the dynamic and volume coefficients of viscosity. When considering ferrofluids, η shows a nonlinear dependence with the magnetic field [78]. Applications involving unequilibrated ferrofluid solutions (i.e., those for which $\boldsymbol{M} \times \boldsymbol{H} \neq 0$) should incorporate the effects resulting from particle rotation in a viscous carrier liquid. An additional term should be added to the viscous stress tensor T_ν, and the angular momentum and magnetic relaxation equations should be considered [75,77].

The structure of the magnetic tensor reflects the complete analogy between magnetostatics and electrostatics [47]. The electric interaction has been widely studied in the context of two-phase flows [28] and does not have a significant incidence for the applications discussed in this work. Even though the small differential electrode potential (≈1.5 V) produces an electric field, the associated electric force is several orders of magnitude weaker than its magnetic counterpart, as shown in Sec. V.A. Consequently, this discussion focuses on the magnetohydrodynamic effect by assuming an electrically neutral medium that remains in thermodynamic equilibrium with constant density, temperature, and chemical potentials. A separate analysis is presented in Sec. V.B for charge-carrying electrolytes, where the Lorentz force becomes dominant. After dropping the electric terms, the stress tensor becomes

$$\mathrm{T} = \mathrm{T}_p + \mathrm{T}_\nu + \mathrm{T}_m \tag{7}$$

This formulation does not implement any assumption regarding the constitutive relation of the material. In some cases, however, it may be useful to particularize the analysis to linear media, as presented in Ref. [47]. Linear electric results are given in Ref. [28] and can be easily adapted to the dia/paramagnetic case by making use of the analogy between magnetostatics and electrostatics.

1. Body Force Distributions

The forces per unit volume exerted on the medium in the absence of electric fields can be computed as the divergence of the stress tensor given by Eq. (7), resulting in [75]

$$\boldsymbol{f}^V = \nabla \cdot \mathrm{T} = \boldsymbol{f}_p^V + \boldsymbol{f}_\nu^V + \boldsymbol{f}_m^V \tag{8}$$

with

$$\boldsymbol{f}_p^V = \nabla \cdot \mathrm{T}_p = -\nabla p^* \tag{9a}$$

$$\boldsymbol{f}_\nu^V = \nabla \cdot \mathrm{T}_\nu = \nabla \cdot \left\{\eta[\nabla \boldsymbol{v} + (\nabla \boldsymbol{v})^T] + \lambda(\nabla \cdot \boldsymbol{v})\boldsymbol{I}\right\} \tag{9b}$$

$$\boldsymbol{f}_m^V = \nabla \cdot \mathrm{T}_m = \mu_0 M \nabla H \tag{9c}$$

If the viscosity coefficients η and λ, are considered constant, the viscous term reduces to

$$\boldsymbol{f}_\nu^V = \eta \nabla^2 \boldsymbol{v} + (\eta + \lambda)\nabla(\nabla \cdot \boldsymbol{v})$$

2. Boundary Conditions

Surface forces appear in the interface between immiscible media as a consequence of the discontinuity in the stress tensor. Those forces are balanced according to the condition of stress equilibrium, leading to [75]

$$\boldsymbol{t}_{n,2} - \boldsymbol{t}_{n,1} = 2\sigma\mathcal{H}\boldsymbol{n}_1 \tag{10}$$

where $\boldsymbol{t}_{n,i} = \boldsymbol{n}_i \cdot \mathrm{T}_{m,i}$ is the stress vector, $\boldsymbol{n}_i$ is the external normal of the medium i, the right term is the capillary pressure, σ is the surface tension, and $\mathcal{H}$ is the arithmetic mean curvature of the interface. Implementing the magnetic, viscous stress tensor given by Eq. (7), the stress vector is expressed as

$$\boldsymbol{t}_n = -p^*\boldsymbol{n} + \eta\left[2\frac{\partial v_n}{\partial x_n}\boldsymbol{n} + \left(\frac{\partial v_n}{\partial x_t} + \frac{\partial v_t}{\partial x_n}\right)\boldsymbol{t}\right] + \lambda(\nabla \cdot \boldsymbol{v})\boldsymbol{n} - \frac{\mu_0}{2}H^2\boldsymbol{n} + B_n\boldsymbol{H} \tag{11}$$

where v_n and v_t are the normal and tangential velocity components, and x_n and x_t the distances along the normal and tangential directions, respectively. Computing the balance at the interface, considering Gauss's and Ampre's laws, and expressing the result in the normal (n) and tangential (t) directions, the ferrohydrodynamic (FHD) viscous boundary condition is obtained [75]:

$$n\text{:}\left[p^* - 2\eta\frac{\partial v_n}{\partial x_n} - \lambda(\nabla \cdot \boldsymbol{v}) + p_n\right] + 2\sigma\mathcal{H} = 0 \tag{12a}$$

$$t\text{:}\left[\eta\left(\frac{\partial v_n}{\partial x_t} + \frac{\partial v_t}{\partial x_n}\right)\right] = 0 \tag{12b}$$

with $p_{n,i} = \mu_0 M_{n,i}^2/2$ being a pressure-like term named *magnetic normal traction*, and the brackets denoting a difference across the interface. If the second medium is nonmagnetic and viscosity is neglected, the normal balance reduces to the inviscid boundary condition between magnetizable and nonmagnetizable media obtained in Ref. [78], as it should.

C. Effective Total Forces

As shown in Ref. [79], different equivalent formulations can be employed to compute the total magnetic force experienced by a body. One of the most common procedures consists of integrating the volume and surface magnetic force densities as

$$\boldsymbol{F}_m = \int_V \mathrm{d}V \boldsymbol{f}_m^V + \oint_{\partial V} \mathrm{d}S \boldsymbol{f}_m^S \tag{13}$$

where V and ∂V denote the volume and surface of a magnetized medium, respectively. The surface force distribution is generated by the discontinuity of the imanation field, and the volume force distribution is obtained by the well-known Kelvin force expression given in Eq. (9c). In the case of a magnetic body b surrounded by a magnetic environment me, Eq. (13) may be reformulated by integrating the environmental pressure on the interface. After considering the quasi-static momentum balance arising from Eq. (1b), the effective total magnetic force results to be

$$\boldsymbol{F}_m^{\mathrm{eff}} = \int_V \mathrm{d}V \boldsymbol{f}_m^{V,\mathrm{eff}} + \oint_{\partial V} \mathrm{d}S \boldsymbol{f}_m^S \tag{14}$$

where the surface force distribution in ∂V is only due to the discontinuity of the imanation field

$$\boldsymbol{f}_m^S = \frac{\mu_0}{2}\left(M_{n,b}^2 - M_{n,\mathrm{me}}^2\right)\boldsymbol{n} \tag{15}$$

with $\boldsymbol{n}$ being the external normal of the body surface ∂V. The effective volume force distribution in V is

$$\boldsymbol{f}_m^{V,\mathrm{eff}} = \mu_0\left(\chi_b^{\mathrm{vol}} H\nabla H - \chi_{\mathrm{me}}^{\mathrm{vol}} H^*\nabla H^*\right) \tag{16}$$

where H^* is the virtual magnetic field that would be present if the volume V was occupied by the environment. The same expression can be obtained by applying the Archimedes's principle.

If the system is in thermodynamic equilibrium, the total force can be also computed by integrating the magnetic stress force in the external contour ∂V^+ [79]. Taking again into account the Archimedes's principle, the effective magnetic force acting on the magnetic medium b can be formulated as

$$\boldsymbol{F}_m^{\mathrm{eff}} = \oint_{\partial V} \mathrm{d}S\boldsymbol{n} \cdot [\mathrm{T}_m^+ - (\mathrm{T}_m^*)^+] \tag{17}$$

where T_m^+ is the magnetic stress tensor in the external contour ∂V^+ when the volume V is occupied by the medium b, and $(\mathrm{T}_m^*)^+$ is the magnetic stress tensor at the same points computed as if the volume V was part of the environment.

A third equivalent formulation of the effective magnetic force can be obtained by applying the principle of virtual works to the free energy variation of a magnetizable medium caused by changes in the applied magnetic field $\boldsymbol{H}_0$. The result is a well-know magnetic force expression [47,76,79] that after considering the surrounding medium becomes

$$\boldsymbol{F}_m^{\mathrm{eff}} = \mu_0 \int_V \mathrm{d}V\left[\left(\chi_b^{\mathrm{vol}}\boldsymbol{H} - \chi_{\mathrm{me}}^{\mathrm{vol}}\boldsymbol{H}^*\right) \cdot \nabla\right]\boldsymbol{H}_0 \tag{18}$$

The previous expressions constitute the formulation of the Archimedes's principle for the magnetic component of the external fields. The effective electric and inertial forces can be obtained by following the same procedure, with the latter being given by

$$\boldsymbol{F}_{\mathrm{in}}^{\mathrm{eff}} = \int_V \mathrm{d}V(\rho_b - \rho_{\mathrm{me}})\boldsymbol{g} \tag{19}$$

D. Magnetic Susceptibility

The magnetic susceptibility is an intrinsic property of the medium that defines the relation between the fields $\boldsymbol{M}$ and $\boldsymbol{H}$, which are aligned in soft magnetic materials. Diamagnetic and paramagnetic substances generally have small and constant volume susceptibility values. Ferrofluids, on the contrary, are characterized by large susceptibilities and a nonlinear dependence between $\boldsymbol{M}$ and $\boldsymbol{H}$. Magnetic susceptibilities are commonly expressed per unit volume (χ^{vol}), mass (χ^{mass}), or mole (χ^{mol}) in the international or CGS systems [80].

Because KOH and NaOH solutions are widely employed in water electrolysis technologies, a brief analysis of their magnetic suscep-

Table 1 Relevant magnetic parameters of alkaline electrolytes expressed in the CGS system [81,82]

Solute	$\mathcal{M}_{\text{solute}}$, g/mol	$\chi^{\text{mol}}_{\text{cation}}/10^{-6}$, cm^3/mol	$\chi^{\text{mol}}_{\text{OH}^-}/10^{-6}$, cm^3/mol	$\chi^{\text{mass}}_{\text{H}_2\text{O}}/10^{-6}$ [cm^3/g]
NaOH	39.9971	−6.8	−12	−0.720
KOH	56.1056	−14.9		

tibility is here presented. Assuming that dipole–dipole interactions are negligible, Wiedemann's additivity law states that

$$\chi^{\text{mass}}_{\text{sol}} = \sum_{i=1}^{N} p_i \chi^{\text{mass}}_i \tag{20}$$

where $\chi^{\text{mass}}_{\text{sol}}$ is the mass susceptibility of the solution, and p_i is the mass fraction of each substance. Equivalent expressions are found for volume and molar susceptibilities [80]. The magnetic susceptibility of diluted salts can be computed as [81]

$$\chi^{\text{mass}}_{\text{salt}} = \frac{\chi^{\text{mol}}_{\text{cation}} + \chi^{\text{mol}}_{\text{anion}}}{\mathcal{M}_{\text{salt}}} \tag{21}$$

with $\mathcal{M}_{\text{salt}}$ being the molar mass of the salt. The susceptibilities of the ions are expressed per unit mole, as commonly reported in the literature. Values for KOH and NaOH solutions are given in Table 1.

The approximate evolution of the magnetic susceptibility of KOH and NaOH solutions with the solute mass fraction is reported in Fig. 3, where the solubility of the solutions is taken from Ref. [83] at 25°C and a constant solution volume is assumed. Because the magnetic force is directly proportional to the magnetic susceptibility, this result implies that liquid electrolytes are particularly well suited for magnetic buoyancy applications, with increases of magnetic susceptibility of up to an 80%. Because PEM cells employ deionized water in contact with the electrodes, the magnetic susceptibility of water should be employed in the calculations.

IV. Bubble Dynamics

The magnetic buoyancy force can produce significant effects in the generation and evolution of gas bubbles over electrodes or boiling surfaces. Such effects have been observed in experiments involving electric fields [27] and ferrofluids subject to magnetic fields [48,49]. In consequence, understanding this process is of major importance for future applications.

The evolution of an isolated gas bubble subject to an inhomogeneous magnetic field in microgravity can be studied as a four-step process, represented in Fig. 4: nucleation, growth, detachment, and transport. The magnetic force should not produce significant effects

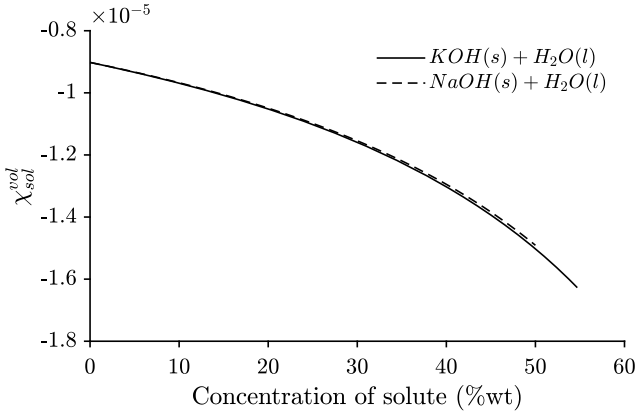

Fig. 3 Volume magnetic susceptibility of KOH and NaOH solutions as a function of the mass fraction of solute neglecting dipole interaction.

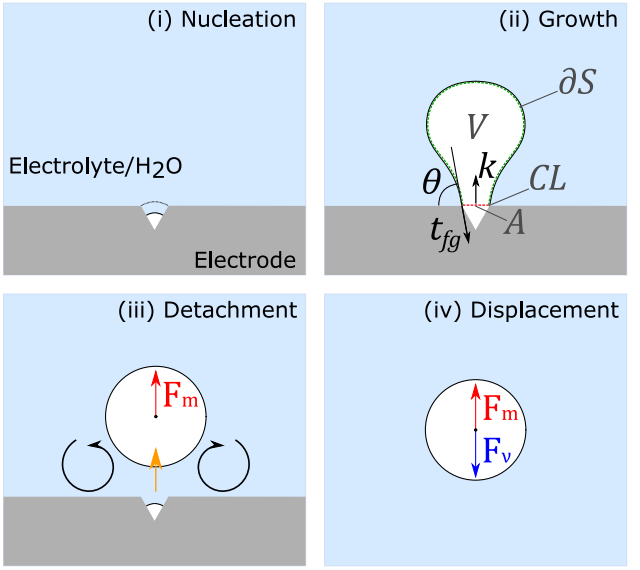

Fig. 4 Conceptual stages of single bubble evolution when subject to an inhomogeneous magnetic field in microgravity.

in the nucleation phase, but may impact the rest. Detachment occurs when the vertical momentum balance is no longer satisfied, inducing a microconvection flow in the surrounding liquid. The bubble subsequently accelerates until viscous drag $\boldsymbol{F}_\nu$ compensates the magnetic buoyancy force, reaching the terminal velocity. Although microgravity experiments show that the actual electrolysis reaction is significantly more complicated due to the formation of a layer of bubbles and their coalescence [13–16], the tools here introduced are still useful to draw fundamental conclusions. A comprehensive chemical analysis of the bubble nucleation process can be found in Ref. [84].

A. Growth

The quasi-static momentum balance is one of the fundamental and most widely extended tools to study bubble growth. Let us consider a liquid environment with density ρ_f and a body consisting on a single gas bubble with volume V, density ρ_g, and surface tension σ. The bubble is sitting on an horizontal electrode with apparent contact angle θ while subject to an inertial acceleration $\boldsymbol{g}$. In the absence of dynamic forces, the momentum balance can be obtained as done in Ref. [28] for the electric interaction, resulting in

$$\int_V \mathrm{d}V \rho_g \boldsymbol{g} + \int_{\text{CL}} \mathrm{d}L \sigma \boldsymbol{t}_{fg} + \oint_{\partial V} \mathrm{d}S \boldsymbol{n} \cdot \mathrm{T}^+_p + \oint_{\partial V} \mathrm{d}S \boldsymbol{n} \cdot \mathrm{T}^+_m = 0 \tag{22}$$

where CL denotes the circular contact line of diameter D_0, and $\boldsymbol{t}_{\text{fg}}$ is the tangent unit vector in the meridian plane. It should be noted that ∂V, which can be decomposed as a surface ∂S on the liquid face of the gas–liquid interface and surface A delimited by the contact line (CL) in the gas region, denotes a complete surface enclosing the pinned bubble volume V. The pressure term can be expanded as

$$\oint_{\partial V} \mathrm{d}S \boldsymbol{n} \cdot \mathrm{T}^+_p = -\oint_{\partial V} \mathrm{d}S p^*_f \boldsymbol{n} + \int_A \mathrm{d}S (p^*_f - p_g) \boldsymbol{n} \tag{23}$$

where p^*_f is the virtual composite pressure applied to the magnetic fluid if it occupied the bubble volume V. The term $(p^*_f - p_g)$ is the virtual fluid overpressure with respect to the gas flow pressure evaluated at the plane A. In quasi-static conditions, the first term in the right equals the inertial and magnetic floatability forces acting on the bubble, and Eq. (22) can be reformulated as

$$\int_{\text{CL}} \mathrm{d}L \sigma \boldsymbol{t}_{fg} + \int_A \mathrm{d}S (p^*_f - p_g) \boldsymbol{n} + \boldsymbol{F}^{\text{eff}}_{\text{in}} + \boldsymbol{F}^{\text{eff}}_m = 0 \tag{24}$$

where $\boldsymbol{F}_{\text{in}}^{\text{eff}}$ is defined by Eq. (17), and $\boldsymbol{F}_{m}^{\text{eff}}$ is given by Eq. (14) or, equivalently, Eq. (18) or Eq. (19). For practical purposes, it is useful to project Eq. (24) on an axis $\boldsymbol{k}$ perpendicular to A, which results in

$$F_b + F_p + F_\sigma + F_m = 0 \tag{25}$$

with the buoyancy, internal overpressure, surface tension, and magnetic forces being given by

$$F_b = \boldsymbol{k} \cdot \boldsymbol{F}_{\text{in}}^{\text{eff}} \approx V(\rho_g - \rho_f)\boldsymbol{k} \cdot \boldsymbol{g} \tag{26}$$

$$F_p = \frac{\pi D_0^2}{4}(p_g - p_f^*) \tag{27}$$

$$F_\sigma = \int_{\text{CL}} \mathrm{d}L\sigma \boldsymbol{k} \cdot \boldsymbol{t}_{fg} \approx -\pi D_0 \sigma \sin\theta \tag{28}$$

$$F_m = \boldsymbol{k} \cdot \boldsymbol{F}_m^{\text{eff}} \tag{29}$$

and where uniform fluid density and overpressure on A have been assumed. For water–gas solutions, with susceptibilities of the order of $|\chi^{\text{vol}}| \approx 10^{-6}$, the magnetic fields in Eq. (18) can be approximated as $\boldsymbol{H}, \boldsymbol{H}^* \approx \boldsymbol{H_0}$. The total force exerted on a small, spherical gas bubble is then

$$\boldsymbol{F}_m^{\text{eff}} \approx \frac{2}{3}\pi R_b^3 \mu_0 \Delta\chi^{\text{vol}} \nabla H_0^2 \tag{30}$$

where R_b is the radius of the bubble and $\Delta\chi^{\text{vol}} = \chi_b^{\text{vol}} - \chi_{\text{me}}^{\text{vol}}$ denotes the differential magnetic susceptibility between gas and the water environment. This approach has been employed in previous works on dielectric manipulation in low gravity [53,54]. For the quasi-axisymmetric case, Eq. (29) can be then approximated by

$$F_m \approx \frac{2}{3}\pi R_b^3 \mu_0 \Delta\chi^{\text{vol}} \frac{\partial H_0^2}{\partial z} \tag{31}$$

The momentum balance may consider a forced viscous shear flow by including the viscous stress tensor and its associated lift and drag expressions [85].

B. Detachment

The detachment of the bubble is produced when the balance of vertical forces cannot longer be satisfied with increasing volume [27]. In this context, the magnetic force F_m can be employed to accelerate the detachment process or, equivalently, reduce the critical bubble volume.

Alternative simplified expressions can be developed to estimate the bubble detachment radius. In boiling and heat transfer research, the maximum break-off diameter of a bubble on an upward facing surface is usually estimated form Fritz's equation [86]

$$d_0 = 1.2\theta\sqrt{\frac{\sigma}{g(\rho_f - \rho_g)}} \tag{32}$$

If the bubble is sufficiently small, the magnetic force may be approximated by a constant, uniform field. The magnetic Fritz equation would then be rewritten as

$$d_0 = 1.2\theta\sqrt{\frac{\sigma}{f_m + g(\rho_f - \rho_g)}} \tag{33}$$

with $f_m = F_m/V$ being the overall magnetic body force density (in N/m^3). The departure diameter may deviate from this result due to the microconvection flow associated to the detachment process [86] and the interactions between adjacent bubbles [13,14,16]. Furthermore, in electrolysis applications the break-off diameter also depends on the surface current density through an expression of the form [87]

$$\frac{d_b}{d_0} = \left(1 + k_1 \frac{I/A}{[A/m^{-2}]}\right)^{-k_2} \tag{34}$$

where k_i are fitting parameters, I is the electrode current intensity, and A is the effective surface of the electrode.

C. Displacement

The movement of a spherical bubble within a liquid can be described by the balance between buoyancy and viscous forces

$$m_b{}' \frac{d^2\boldsymbol{x}}{dt^2} = \boldsymbol{F}_m^{\text{eff}} + \boldsymbol{F}_{\text{in}}^{\text{eff}} + \boldsymbol{F}_R \tag{35}$$

with $m_b{}' = (4/3)\pi R_b^3(\rho_g + 0.5\rho_f)$ being the virtual mass of the bubble [88], and $\boldsymbol{F}_R = -6\pi R_b \eta(d\boldsymbol{x}/dt)$ the viscous drag according to Stokes' law ($Re \ll 1$). By making use of the simplified total force expression given by Eq. (30), the momentum balance is reduced to

$$\left(\rho_g + \frac{1}{2}\rho_f\right)\frac{d^2\boldsymbol{x}}{dt^2} \approx \frac{\mu_0}{2}\Delta\chi^{\text{vol}}\nabla H_0^2 + (\rho_g - \rho_f)\boldsymbol{g} - \frac{9\eta}{2R_b^2}\frac{d\boldsymbol{x}}{dt} \tag{36}$$

Small gas bubbles experience large accelerations due to their low density, rapidly reaching a steady-state dynamic regime. This justifies the employment of the terminal velocity, defined as the steady-state velocity of the bubble, as a physically meaningful parameter. The terminal velocity can be derived from Eq. (36), resulting in

$$\boldsymbol{v}_t \approx \frac{2R_b^2}{9\eta}\left[\frac{\mu_0}{2}\Delta\chi^{\text{vol}}\nabla H_0^2 + (\rho_g - \rho_f)\boldsymbol{g}\right] \tag{37}$$

The validity of this expression is limited to small bubbles and low-susceptibility gases and liquids. Similar formulations can be found in the literature [51,53].

V. Numerical Analysis

A series of numerical results are here presented to better understand low-gravity magnetic buoyancy and its applications in electrolysis and phase separation. This preliminary analysis and system sizing is made based on the previously introduced expressions. For this purpose, an N52 neodymium magnet, one of the strongest categories commercially available, is considered. The magnet is characterized by a magnetization of 1150 kA/m. Relevant physicochemical properties of water, gas hydrogen, and gas oxygen at 25°C and 1 atm are given in Table 2.

A. Electrically Neutral Media

The effects of magnetic buoyancy on electrically neutral media, which are the main subject of this work, are first addressed. This includes pure water in contact with the external face of PEM electrodes and alkaline electrolytes outside the OH^- transport region. Although in the second case the presence of charged electrodes leads to a local distribution of charge, the Debye length [89] of such distribution becomes about 0.1 nm for NaOH and KOH solutions in water in standard conditions. That is, the alkaline electrolyte outside the OH^- transport region can be considered electrically neutral, and hence unaffected by Lorentz's electric and magnetic force terms.

Table 2 Relevant physicochemical properties of water, gas hydrogen, and gas oxygen at 25°C and 1 atm [83]

Material	$\mathcal{M}$, g/mol	ρ, kg/m^3	χ^{vol}	η, Pa · s
H_2O (l)	18.015	997	$-9.1 \cdot 10^{-6}$	0.0009
H_2 (g)	2.016	0.082	$1 \cdot 10^{-10}$	— —
O_2 (g)	31.999	1.308	$3.73 \cdot 10^{-7}$	— —

To illustrate the magnetic buoyancy concept, the volume force density $f_m^{V,\text{eff}}$ [Eq. (16)] is first computed by means of finite-element simulations in Comsol Multiphysics. The equations and boundary conditions of the magnetic model are similar to the ones employed in Ref. [60]. Figure 5 represents the radial cross section of the volume force density field induced by a cylindrical magnet with 1 cm radius and 0.5 cm height in a O_2 bubble. Because of the small magnetic susceptibility of water, values of 1 nN/mm^3, corresponding to an inertial acceleration of $\approx$1 mm/s^2, are reached at 2 cm from the surface of the magnet. In contrast, an hypothetical square PEM cell with an electrode surface of 2 cm^2 and a potential difference of 1.2 V exerts a dielectric force of 10^{-5}–10^{-1} nN/mm^3 on a gas bubble sitting on the electrode. It is then justified to neglect the dielectric force for the applications here considered.

Figure 6 shows the terminal velocity field [Eq. (37)] of a 1-mm-radius O_2 bubble immersed in water and subject to the influence of a permanent neodymium magnet in microgravity ($g \approx 0$). The red arrows, solid lines, and dashed lines correspond to the nonscaled velocity vector, the constant velocity contours, and the magnetic flux lines, respectively. Three different cylindrical magnets magnetized along the axis are studied, the first (a) with 10 mm radius and 5 mm height, the second (b) with 20 mm radius and 5 mm height, and the third (c) with 10 mm radius and 20 mm height. The velocity vectors point toward the magnets, which adopt the role of a bubble sink. This effect can be employed to induce phase separation and the detachment of gas bubbles from an electrode or boiling surface in microgravity. The performance of the magnets is hampered by the rapid magnetic field decay, leading to terminal velocities of the order of 1 mm/s at approximately 15 mm from their surface. Larger velocities are experienced in the corners of the magnets, where the magnetic field gradient is maximum.

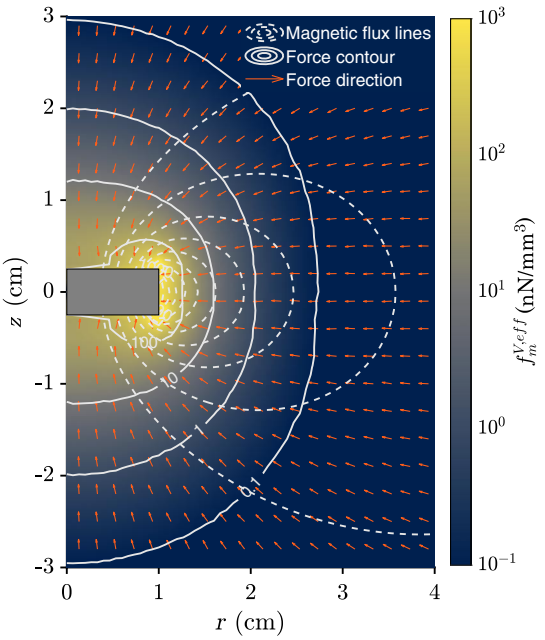

Fig. 5 Radial cross section of the magnetic force density induced by a cylindrical magnet in an O_2 gas bubble.

The magnetic body force is proportional to the gradient of the magnetic field $\boldsymbol{H}$ and its module. When a quasi-uniform field is generated, as observed near the axis of Fig. 6b, the magnetic forces and terminal velocities are reduced. It is then convenient to select a magnetic configuration that maximizes the force exerted on the bubbles. Similar problems appear in biomedical applications dealing with magnetic drug delivery and targeting [90–93] or magnetic resonance imaging [94,95], and have been faced by means of Halbach magnet arrays. A Halbach magnet array is an arrangement of permanent magnets that reinforces the magnetic field on one side of the array and cancels it on the other [96]. These characteristics are convenient for space applications, where the performance of the magnet should be maximized, and its electromagnetic interference and mass should be minimized.

Figure 7 represents a linear array of five $1 \times 1 \times 0.5$ cm^3 neodymium magnets configured considering a) aligned magnetizations and b) Halbach-oriented magnetizations. As in Fig. 6, the terminal velocity map computed with Eq. (37) is represented. It can be observed how the Halbach configuration produces an asymmetrical magnetic field and a more homogeneous terminal velocity distribution, with the 1 mm/s contour line staying at approximately 2 cm from the magnets along the x axis. However, the terminal velocity is shown to decay faster than in the linear configuration, as exemplified by the 0.1 mm/s line. This characteristic may guide the design of future phase separators. For instance, the linear configuration may be more suitable for the gas collection process due to the convergence of the velocity vectors toward the extremes of the magnet, whereas the Halbach array may produce a more homogeneous magnetic force distribution over the electrodes.

These results can be easily extended to the KOH and NaOH solutions studied in Sec. III.D by noting the linear dependence of

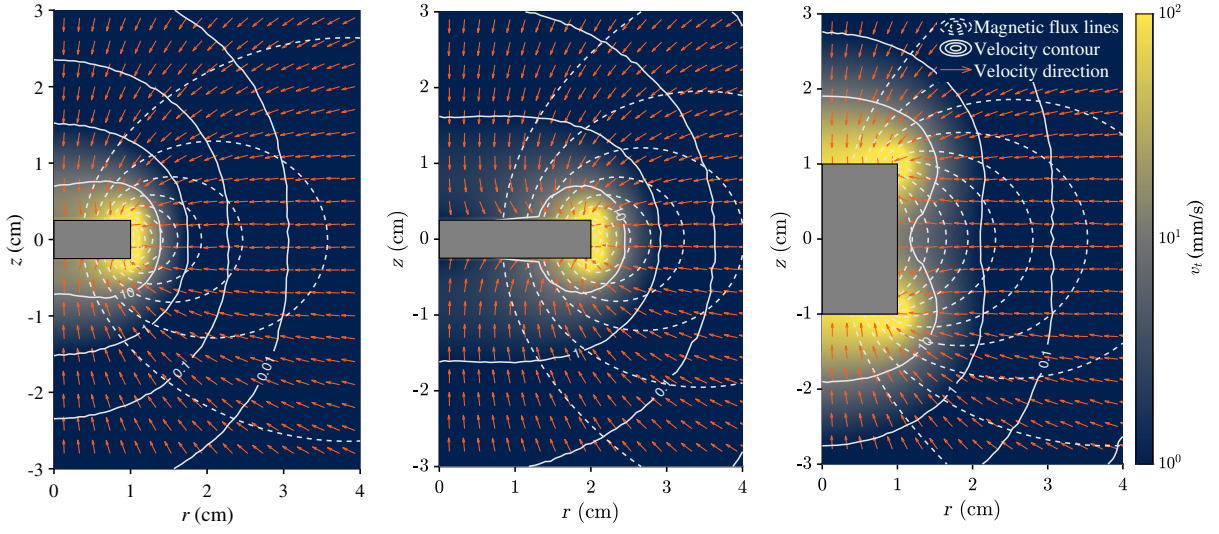

a) Base configuration **b) Radially extended** **c) Axially extended**

Fig. 6 Radial cross section of the microgravity terminal velocity v_t induced by a cylindrical magnet in an O_2 gas bubble with 1 mm radius in water.

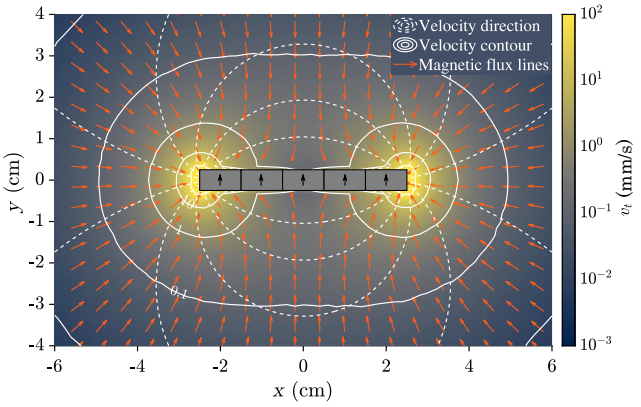

a) Uniform magnetization

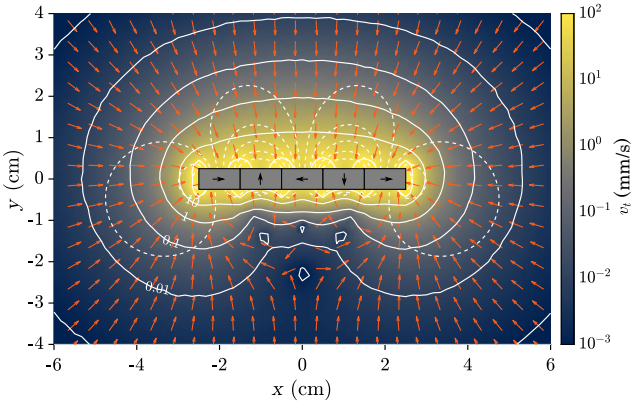

b) Halbach array

Fig. 7 Two-dimensional simulation with 1 cm depth of the microgravity terminal velocity v_t induced by an array of magnets in an O_2 gas bubble with 1 mm radius in water. The black arrows denote the magnetization direction.

the terminal velocity with the volume magnetic susceptibility χ^{vol}. Because this parameter is a 60–80% larger than that of pure water, the performance of the system would be greatly improved. Similar effects would be observed in applications involving ferrofluids, whose magnetic susceptibility can be of the order 10. Without considering the many technical difficulties associated with their operation, such technologies could easily reach magnetic force values equal or larger than the acceleration of gravity. This may lead to large improvements in the productivity of the cell both on Earth and in space.

A second effect on interest arising from the application of an inhomogeneous magnetic field to a nucleation surface is the potential reduction of the break-off diameter. This is explored in Fig. 8 for an isolated bubble by making use of Eq. (33). A 10-mm-radius, 5-mm-height cylindrical magnet is considered in microgravity, assuming a contact angle of $\theta = 5°$. The magnetic Fritz equation predicts a reduction of the break-off diameter from 10 cm to few millimeters as the bubble approaches the magnet. Without considering the variations in contact angle and surface tension, the employment of saturated KOH/NaOH solutions would reduce the diameter by a 25% due to the increase in magnetic susceptibility. On the other hand, no significant differences are observed between O_2 or H_2 gas bubbles due to their small magnetic susceptibility. These predictions should, however, be taken with care, as the magnetic Fritz equation assumes an homogeneous magnetic force in the bubble volume, and this assumption is being violated in a significant portion of the solution domain. Even if this was not the case, the Fritz equation describes the detachment of an isolated bubble. Experimental observations have shown that the break-off diameter in microgravity is actually much smaller due to the interaction between bubbles located in the first layer over the electrodes [13,14,16]. Numerical simulations based on the framework of analysis presented in Sec. IV.A and experimental results are then required to shed light on this problem.

Nonmagnetic cell components have been considered throughout this discussion. However, electrodes and bipolar plates are made of diamagnetic (carbon), paramagnetic (titanium), or ferromagnetic (nickel, ferritic stainless steel) materials. Those from the third group, with relative permeabilities up to 2000, can be strongly magnetized by external fields and modify significantly their local magnetic force distributions. If not taken into consideration, these disturbances may lead to the undesired accumulation of bubbles at the surface of the electrodes. Although the local effect needs to be evaluated in a case-by-case basis, it can become important for massive, ferromagnetic electrodes subject to strong magnetic fields. In particular, corner geometries will tend to generate magnetic singularities, leading to the generation of bubble sinks (as it happens in the well-known lightning rod effect [97]).

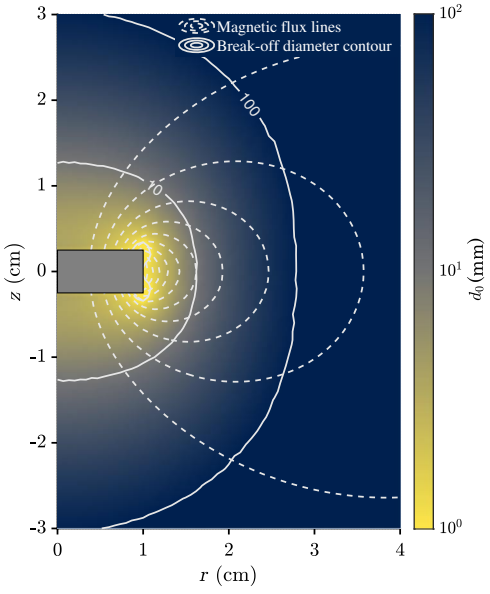

a) Break-off diameter distribution

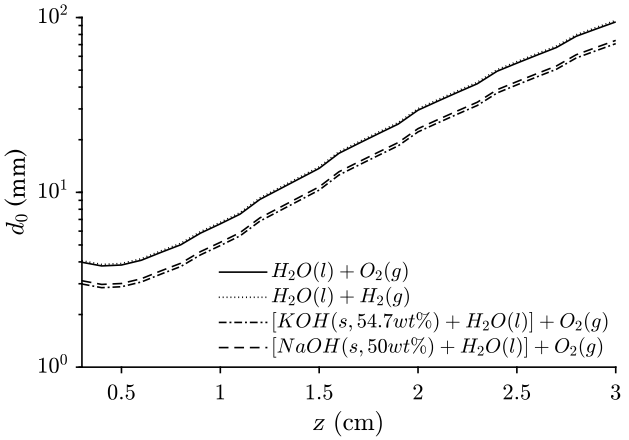

b) Break-off diameter in axis of symmetry

Fig. 8 a) Radial cross section of the break-off diameter d_0 induced by a 10-mm-radius, 5-mm-height cylindrical magnet in an O_2 gas bubble in water with $\theta = 5°$. b) Break-off diameter in the axis of symmetry for different gas–liquid combinations.

B. Effect of Magnetic Field in Unbalanced Electrolyte

Lorentz's force must be considered when an electromagnetic field is applied to unbalanced electrolyte solutions, adopting the form

$$\mathcal{L} = \rho_V \boldsymbol{E} + \boldsymbol{J}_e \times \boldsymbol{B} \tag{38}$$

As with the diamagnetic force, a buoyancy effect is induced on the gas bubbles. In PEM electrolysis the only volume where there is a charge unbalance is the membrane itself, where a highly acidic medium is created in the presence of water. Assuming a current density of 1 A/cm^2, a magnetic field of 1 T, a potential difference between electrodes of 1.2 V, and a membrane thickness of 100 μm in an acidic solution with pH 1, the electric term dominates over the magnetic term by a factor 10^7. This factor increases for more acidic solutions, so it can be concluded that the imposed magnetic field has virtually no effect in the solid electrolyte.

As for alkaline electrolysis, previous works have reported the effects of an external magnetic field in the productivity of alkaline cells when such field is applied to the OH^- transport region [62,63,65,66,69]. For instance, the setup depicted in Fig. 9 employs two parallel flat electrodes immersed in an alkaline electrolyte to which a constant magnetic field is imposed. The magnetic field is applied parallel to the plane of the electrode, and because the mean electric current density vector $\boldsymbol{J}_e$ is perpendicular to such electrode, a vertical force is induced by the magnetic term in Eq. (38). With a current density of 0.5 A/cm^2 and a characteristic magnetic field of 1 T, a Lorentz buoyancy force of 5000 nN/mm^3 would be generated. This term is several orders of magnitude larger than the diamagnetic force studied in Sec. V.A and could lead to interesting low-gravity applications. However, the need to generate gas bubbles between the electrodes may raise safety concerns in space applications, where the recombination of products represents a critical safety hazard. Such bubbles would also modify the local current flow, leading to more complex microfluidic interactions arising from a nonuniform Lorentz force distribution [98,99].

C. Scale-Up Process

Many times innovations at the subcell or cell levels do not survive the scale-up process from a single-cell to full-size stack. It is then convenient to give some hints on how such process should be carried out for the diamagnetic cell architectures here introduced.

Two main scale-up strategies may be followed: either a continuous magnetic sheet with Halbach-like arrays (like the one represented in Fig. 7b) is located in parallel to the electrodes, or a series of magnets are strategically positioned to collect the bubbles. In both cases, the magnetic system can be adapted to any cell surface. However, the second approach leads to important mass savings. This is shown in Fig. 10, where a 1 kg array of twelve $1 \times 1 \times$ 10 cm^3 magnets is employed to induce diamagnetic buoyancy at the surface of three 100 cm^2 PEMs. The hypothetical location of the membrane electrode assemblies is represented by light-gray areas. Black arrows, red arrows, and solid lines represent the magnetization direction, nonscaled velocity vector, and constant velocity contours, respectively. The bubble velocity vectors point toward the magnets, which can be used as gas collection points. This design can be largely improved by optimizing the distribution of magnets in the z axis, or by employing anode- and cathode-feed PEM architectures where only one side of the membrane requires phase separation.

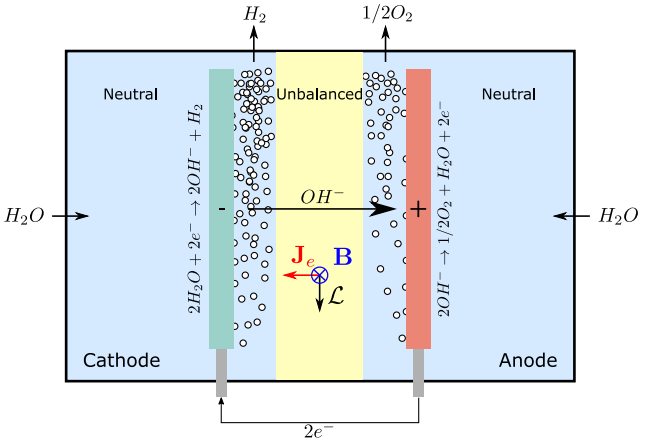

Fig. 9 Alkaline cell where the charge unbalance in the OH^- transport region leads to a magnetic Lorentz buoyancy effect in the presence of an out-of-plane magnetic field $\boldsymbol{B}$.

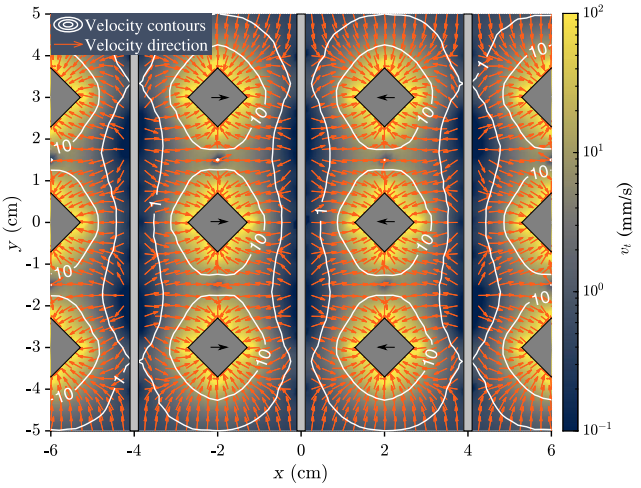

Fig. 10 Two-dimensional simulation with 10 cm depth of the microgravity terminal velocity v_t induced by an array of magnets in an O_2 gas bubble with 1 mm radius in water.

In addition to selecting an efficient magnetic architecture, the movement of the bubbles should be constrained by means of an optimized wall (or bipolar plate) profile. Such profile would be adapted to the magnetic force potential to push the bubbles toward specific collection points, where the gas is finally extracted. Hydrophobic and hydrophilic surfaces may be employed to induce the accumulation and coalescence of bubbles.

VI. Conclusions

The applications of diamagnetic buoyancy in low-gravity electrolysis, boiling, and phase separation have been introduced. The diamagnetic force can be employed to induce the early detachment of gas bubbles from the electrodes, increasing the effective surface area and effectively separating the phases. A comprehensive theoretical analysis of the problem has been presented together with simplified expressions that ease preliminary studies.

Numerical simulations are employed to show how modern neodymium magnets induce a significant magnetic force in gas–water flows at distances of the order of 2 cm. The reachability of the system is increased by an 80% when saturated NaOH and KOH electrolytes are considered. For unbalanced alkaline electrolytes, the magnetic term of the Lorentz force can lead to strong magnetic buoyancy forces, an effect that may open interesting avenues for research. Finally, potential approaches to scale up the diamagnetic electrolysis architecture have been suggested.

There are several scientific and technical questions of interest that need to be solved before diamagnetic buoyancy is employed in low-gravity technologies. A nonextensive list includes the characterization of the bubble collection process, the experimental and numerical study of magnetically induced bubble detachment, the development of reliable gas collectors, or the analysis of applications employing ferrofluids, whose larger magnetic susceptibilities and a strong magnetic response would lead to significant increases of the magnetic force, also enabling terrestrial applications.

Appendix: Governing Equations for Incompressible Fluids Subject to Static Magnetic Fields

The magnetic phase separation and bubble detachment concept discussed in this paper can be applied to different electrolysis and boiling technologies. However, most of them share four important characteristics: i) the fluids involved are treated as incompressible, ii) steady magnetic fields are imposed, iii) para/diamagnetic substances are employed, and iv) viscous coefficients are considered constant. It is then useful to particularize Eqs. (1) and (2) to this case.

Under the previous assumptions, the magnetohydrodynamic mass and momentum conservation equations become

$$\nabla \cdot \boldsymbol{v} = 0 \tag{39a}$$

$$\rho \frac{D\boldsymbol{v}}{Dt} = \rho \boldsymbol{g} - \nabla p + \eta \nabla^2 \boldsymbol{v} + \mu_0 M \nabla H \tag{39b}$$

subject to the boundary conditions

$$n: \left[p^* - 2\eta \frac{\partial v_n}{\partial x_n} + p_n \right] + 2\sigma \mathcal{H} = 0 \tag{40a}$$

$$t: \left[\eta \left(\frac{\partial v_n}{\partial x_t} + \frac{\partial v_t}{\partial x_n} \right) \right] = 0 \tag{40b}$$

The steady-state Maxwell's equations in the absence of surface currents are employed to compute the magnetic fields, giving

$$\nabla \cdot \boldsymbol{B} = 0 \tag{41a}$$

$$\nabla \times \boldsymbol{H} = \boldsymbol{J}_e \tag{41b}$$

due to the absence of electric fields. The simplified electric and magnetic boundary conditions at the interface are

$$\boldsymbol{n} \cdot (\boldsymbol{B}_2 - \boldsymbol{B}_1) = 0 \tag{42a}$$

$$\boldsymbol{n} \times (\boldsymbol{H}_2 - \boldsymbol{H}_1) = 0 \tag{42b}$$

Acknowledgments

The authors acknowledge the financial support offered by the La Caixa Foundation (ID 100010434) under agreement LCF/BQ/AA18/11680099 to support the Ph.D. studies of Álvaro Romero-Calvo. The assistance of Isabel Romero Calvo and Morphology Visuals in the formatting of the figures presented in this paper is gratefully acknowledged.

References

[1] de Levie, R., "The Electrolysis of Water," *Journal of Electroanalytical Chemistry*, Vol. 476, No. 1, 1999, pp. 92–93. https://doi.org/10.1016/S0022-0728(99)00365-4

[2] Trasatti, S., "Water Electrolysis: Who First?" *Journal of Electroanalytical Chemistry*, Vol. 476, No. 1, 1999, pp. 90–91. https://doi.org/10.1016/S0022-0728(99)00364-2

[3] Newman, D., "Water Electrolysis Reaction Control System," *Proceedings of the 7th Liquid Propulsion Symposium, Chemical Propulsion Information Agency Publications*, Vol. 72, 1965, pp. 105–114.

[4] Roy, R., "Backwards Runs the Reaction," *Mechanical Engineering*, Vol. 130, No. 4, 2008, pp. 32–36. https://doi.org/10.1115/1.2008-APR-3

[5] Papale, W., and Roy, R., "A Water-Based Propulsion System for Advanced Spacecraft," *Space 2006*, AIAA Paper 2006-7240, 2006, pp. 1–13. https://doi.org/10.2514/6.2006-7240

[6] James, K., Moser, T., Conley, A., Slostad, J., and Hoyt, R., "Performance Characterization of the HYDROS Water Electrolysis Thruster," *Proceedings of the Small Satellite Conference 2015*, Paper SSC15-XI-5, Utah State Univ., Utah, 2015, pp. 1–7, https://digitalcommons.usu.edu/smallsat/2015/all2015/75/.

[7] Doyle, K. P., and Peck, M. A., "Water Electrolysis Propulsion as a Case Study in Resource-Based Spacecraft Architecture (February 2020)," *IEEE Aerospace and Electronic Systems Magazine*, Vol. 34, No. 9, 2019, pp. 4–19. https://doi.org/10.1109/MAES.2019.2923312.

[8] Burke, K., "Small Portable PEM Fuel Cell Systems for NASA Exploration Missions," NASA TM-2005-213994, 2005.

[9] Bents, D., Scullin, V., Chang, B., Johnson, D., and Jakupca, I. J., "Hydrogen-Oxygen PEM Regenerative Fuel Cell Development at the NASA Glenn Research Center," NASA TM-2005-214032, 2005.

[10] Lee, K., "Water Electrolysis for In-Situ Resource Utilization (ISRU)," *AIAA Houston Section Annual Technical Symposium (ATS 2016)*, Paper JSC-CN-35703, 2016, https://ntrs.nasa.gov/citations/20160006359.

[11] Sowers, G. F., and Dreyer, C. B., "Ice Mining in Lunar Permanently Shadowed Regions," *New Space*, Vol. 7, No. 4, 2019, pp. 235–244. https://doi.org/10.1089/space.2019.0002

[12] Millet, P., and Grigoriev, S., "Chapter 2–Water Electrolysis Technologies," *Renewable Hydrogen Technologies*, edited by L. M. Gandía, G. Arzamendi, and P. M. Diéguez, Elsevier, Amsterdam, 2013, pp. 19–41. https://doi.org/10.1016/B978-0-444-56352-1.00002-7

[13] Matsushima, H., Nishida, T., Konishi, Y., Fukunaka, Y., Ito, Y., and Kuribayashi, K., "Water Electrolysis Under Microgravity: Part 1. Experimental Technique," *Electrochimica Acta*, Vol. 48, No. 28, 2003, pp. 4119–4125. https://doi.org/10.1016/S0013-4686(03)00579-6

[14] Matsushima, H., Fukunaka, Y., and Kuribayashi, K., "Water Electrolysis Under Microgravity: Part II. Description of Gas Bubble Evolution Phenomena," *Electrochimica Acta*, Vol. 51, No. 20, 2006, pp. 4190–4198. https://doi.org/10.1016/j.electacta.2005.11.046

[15] Kiuchi, D., Matsushima, H., Fukunaka, Y., and Kuribayashi, K., "Ohmic Resistance Measurement of Bubble Froth Layer in Water Electrolysis Under Microgravity," *Journal of the Electrochemical Society*, Vol. 153, No. 8, 2006, p. E138. https://doi.org/10.1149/1.2207008

[16] Iwasaki, A., Kaneko, H., Abe, Y., and Kamimoto, M., "Investigation of Electrochemical Hydrogen Evolution Under Microgravity Condition," *Electrochimica Acta*, Vol. 43, No. 5, 1998, pp. 509–514. https://doi.org/10.1016/S0013-4686(97)00096-0

[17] Sakurai, M., Shima, A., Sone, Y., Ohnishi, M., Tachihara, S., and Ito, T., "Development of Oxygen Generation Demonstration on JEM (KIBO) for Manned Space Exploration," *44th International Conference on Environmental Systems*, Paper ICES-2014-125, July 2014, pp. 1–7, https://ttu-ir.tdl.org/handle/2346/59644.

[18] Erickson, R. J., Howe, J., Kulp, G. W., and Van Keuren, S. P., "International Space Station United States Orbital Segment Oxygen Generation System On-Orbit Operational Experience," *38th International Conference on Environmental Systems*, Paper 2008-01-1962, 2008. https://doi.org/10.4271/2008-01-1962

[19] Samplatsky, D. J., and Dean, W. C., "Development of a Rotary Separator Accumulator for Use on the International Space Station," *32nd International Conference on Environmental Systems*, SAE TP 2002-01-2360, July 2002. https://doi.org/10.4271/2002-01-2360

[20] Sakurai, M., Terao, T., and Sone, Y., "Development of Water Electrolysis System for Oxygen Production Aimed at Energy Saving and High Safety," *45th International Conference on Environmental Systems*, Paper ICES-2015-273, July 2015, pp. 1–8, https://ttu-ir.tdl.org/handle/2346/64518.

[21] Jenson, R. M., Wollman, A. P., Weislogel, M. M., Sharp, L., Green, R., Canfield, P. J., Klatte, J., and Dreyer, M. E., "Passive Phase Separation of Microgravity Bubbly Flows Using Conduit Geometry," *International Journal of Multiphase Flow*, Vol. 65, Oct. 2014, pp. 68–81. https://doi.org/10.1016/j.ijmultiphaseflow.2014.05.011

[22] Weislogel, M. M., and McCraney, J. T., "The Symmetric Draining of Capillary Liquids from Containers with Interior Corners," *Journal of Fluid Mechanics*, Vol. 859, Jan. 2019, pp. 902–920. https://doi.org/10.1017/jfm.2018.848

[23] Beheshti Pour, N., and Thiessen, D. B., "A Novel Arterial Wick for Gas–Liquid Phase Separation," *AIChE Journal*, Vol. 65, No. 4, 2019, pp. 1340–1354. https://doi.org/10.1002/aic.16499

[24] Beheshti Pour, N., and Thiessen, D. B., "Equilibrium Configurations of Drops or Bubbles in an Eccentric Annulus," *Journal of Fluid Mechanics*, Vol. 863, March 2019, pp. 364–385. https://doi.org/10.1017/jfm.2018.1010

[25] Chipchark, D., "Development of Expulsion and Orientation Systems for Advanced Liquid Rocket Propulsion Systems," USAF TR RTD-TDR-63-1048, Contract AF04 (611)-8200, 1963.

[26] Di Marco, P., and Grassi, W., "Effect of Force Fields on Pool Boiling Flow Patterns in Normal and Reduced Gravity," *Heat and Mass Transfer*, Vol. 45, No. 7, 2009, pp. 959–966. https://doi.org/10.1007/s00231-007-0328-6

[27] Di Marco, P., "Influence of Force Fields and Flow Patterns on Boiling Heat Transfer Performance: A Review," *Journal of Heat Transfer*, Vol. 134, No. 3, 2012, Paper 030801. https://doi.org/10.1115/1.4005146

[28] Di Marco, P., "The Use of Electric Force as a Replacement of Buoyancy in Two-Phase Flow," *Microgravity Science and Technology*, Vol. 24, No. 3, 2012, pp. 215–228. https://doi.org/10.1007/s12217-012-9312-y

[29] Ma, R., Lu, X., Wang, C., Yang, C., and Yao, W., "Numerical Simulation of Bubble Motions in a Coaxial Annular Electric Field Under Microgravity," *Aerospace Science and Technology*, Vol. 96, Jan. 2020, Paper 105525. https://doi.org/10.1016/j.ast.2019.105525

[30] Holder, D. W., O'Connor, E. W., Zagaja, J., and Murdoch, K., "Investigation into the Performance of Membrane Separator Technologies used in the International Space Station Regenerative Life Support Systems: Results and Lessons Learned," *31st International Conference on Environmental Systems*, SAE TP 2001-01-2354, July 2001, pp. 1–13, https://www.sae.org/publications/technical-papers/content/2001-01-2354/. https://doi.org/10.4271/2001-01-2354

[31] Samsonov, N. M., Bobe, L. S., Gavrilov, L. I., Korolev, V. P., Novikov, V. M., Farafonov, N. S., Soloukhin, V. A., Romanov, S. J., Andrejchuk, P. O., Protasov, N. N., Rjabkin, A. M., Telegin, A. A., Sinjak, J. E., and Skuratov, V. M., "Water Recovery and Oxygen Generation by Electrolysis Aboard the International Space Station," *32nd International Conference on Environmental Systems*, SAE TP 2002-01-2358, July 2002. https://doi.org/10.4271/2002-01-2358

[32] Williams, D. E., and Gentry, G. J., "International Space Station Environmental Control and Life Support System Status: 2004–2005," *SAE Transactions*, Vol. 114, Jan. 2005, pp. 64–75.

[33] Williams, D. E., and Gentry, G. J., "International Space Station Environmental Control and Life Support System Status: 2005–2006," *36th International Conference on Environmental Systems*, SAE TP 2006-01-2055, July 2006. https://doi.org/10.4271/2006-01-2055

[34] Williams, D. E., and Gentry, G. J., "International Space Station Environmental Control and Life Support System Status: 2006–2007," *37th International Conference on Environmental Systems*, SAE TP 2007-01-3098, July 2007. https://doi.org/10.4271/2007-01-3098

[35] Takada, K., Velasquez, L. E., Keuren, S. V., Baker, P. S., and McDougle, S. H., "Advanced Oxygen Generation Assembly for Exploration Missions," *49th International Conference on Environmental Systems*, Paper ICES-2019-107, July 2019, https://ttu-ir.tdl.org/handle/2346/84610.

[36] Sakurai, M., Sone, Y., Nishida, T., Matsushima, H., and Fukunaka, Y., "Fundamental Study of Water Electrolysis for Life Support System in Space," *Electrochimica Acta*, Vol. 100, June 2013, pp. 350–357. https://doi.org/10.1016/j.electacta.2012.11.112

[37] Sakurai, M., Terao, T., and Sone, Y., "Development of Water Electrolysis System for Oxygen Production Aimed at Energy Saving and High Safety," *45th International Conference on Environmental Systems*, Paper ICES-2015-273, July 2015, https://ttu-ir.tdl.org/handle/2346/64518.

[38] Sakurai, M., Terao, T., and Sone, Y., "Study on Water Electrolysis for Oxygen Production -Reduction of Water Circulation and Gas-Liquid Separator," *47th International Conference on Environmental Systems*, Paper ICES-2017-215, July 2017, https://ttu-ir.tdl.org/handle/2346/73014.

[39] Sakai, Y., Oka, T., Waseda, S., Arai, T., Suehiro, T., Ito, T., Shima, A., and Sakurai, M., "Development Status of Air Revitalization System in JAXA Closed ECLSS for Future Crew Module," *48th International Conference on Environmental Systems*, Paper ICES-2018-146, July 2018, https://ttu-ir.tdl.org/handle/2346/74127.

[40] Powell, J., Schubert, F., and Jensen, F., "*Static Feed Water Electrolysis Module*," NASA TR CR-137577, 1974.

[41] Schubert, F., Wynveen, R., Jensen, F., and Quattrone, P., "Development of an Advanced Static Feed Water Electrolysis Module," *Proceedings of the Intersociety Conference on Environmental Systems*, ASME Paper 75-ENAS-30, 1975, https://ntrs.nasa.gov/citations/19750056806.

[42] Fortunato, F. A., Kovach, A. J., and Wolfe, L. E., "Static Feed Water Electrolysis System for Space Station Oxygen and Hydrogen Generation," *SAE Transactions*, Vol. 97, Jan. 1988, pp. 190–198.

[43] Powell, J., Schubert, F., and Lee, M., "Impact of Low Gravity on Water Electrolysis Operation," NASA TR CR-185521, 1989.

[44] Davenport, R. J., Schubert, F. H., and Grigger, D. J., "Space Water Electrolysis: Space Station Through Advanced Missions," *Journal of Power Sources*, Vol. 36, No. 3, 1991, pp. 235–250. https://doi.org/10.1016/0378-7753(91)87004-U

[45] Schubert, F., "Electrolysis Performance Improvement Concept Study (EPICS) Flight Experiment-Reflight," NASA TR CR-205554, TR-1415-57, 1997.

[46] Knorr, W., Tan, G., and Witt, J., "The FAE Electrolyser Flight Experiment FAVORITE: Current Development Status and Outlook," *34th International Conference on Environmental Systems*, SAE TP 2004-01-2490, July 2004. https://doi.org/10.4271/2004-01-2490

[47] Landai, L. D., and Lifshitz, E. M., *Electrodynamics of Continuous Media*, edited by L. D. Landai, and E. M. Lifshitz, Vol. 8, 2nd ed., Course of Theoretical Physics, Pergamon Press, Amsterdam, 1984, pp. 105–129, Chap. IV. https://doi.org/10.1016/B978-0-08-030275-1.50010-2

[48] Junhong, L., Jianming, G., Zhiwei, L., and Hui, L., "Experiments and Mechanism Analysis of Pool Boiling Heat Transfer Enhancement with Water-Based Magnetic Fluid," *Heat and Mass Transfer*, Vol. 41, No. 2, 2004, pp. 170–175. https://doi.org/10.1007/s00231-004-0529-1

[49] Abdollahi, A., Salimpour, M. R., and Etesami, N., "Experimental Analysis of Magnetic Field Effect on the Pool Boiling Heat Transfer of a Ferrofluid," *Applied Thermal Engineering*, Vol. 111, Jan. 2017, pp. 1101–1110. https://doi.org/10.1016/j.applthermaleng.2016.10.019

[50] Wakayama, N. I., "Magnetic Buoyancy Force Acting on Bubbles in Nonconducting and Diamagnetic Fluids Under Microgravity," *Journal of Applied Physics*, Vol. 81, No. 7, 1997, pp. 2980–2984. https://doi.org/10.1063/1.364330

[51] Wakayama, N. I., "Utilization of Magnetic Force in Space Experiments," *Advances in Space Research*, Vol. 24, No. 10, 1999, pp. 1337–1340. https://doi.org/10.1016/S0273-1177(99)00743-7

[52] Tillotson, B. J., Torre, L. P., and Houston, J. D., "Method for Manipulation of Diamagnetic Objects in a Low-Gravity Environment," US Patent 6162364, 2000.

[53] Scarl, E., and Houston, J., "Two-Phase Magnetic Fluid Manipulation in Microgravity Environments," *37th Aerospace Sciences Meeting and Exhibit*, AIAA Paper 1999-0844, 1999, pp. 1–5. https://doi.org/10.2514/6.1999-844

[54] Tillotson, B., Houston, J., Tillotson, B., and Houston, J., "Diamagnetic Manipulation for Microgravity Processing," *35th Aerospace Sciences Meeting and Exhibit*, AIAA Paper 19997-0887, 1997, pp. 1–10. https://doi.org/10.2514/6.1997-887

[55] Papell, S., "Low Viscosity Magnetic Fluid Obtained by the Colloidal Suspension of Magnetic Particles," US Patent 3215572, 1963.

[56] Martin, J., and Holt, J., "Magnetically Actuated Propellant Orientation Experiment, Controlling Fluid Motion with Magnetic Fields in a Low-Gravity Environment," NASA TM-2000-210129, M-975, NAS 1.15:210129, 2000.

[57] Marchetta, J. G., "Simulation of LOX Reorientation Using Magnetic Positive Positioning," *Microgravity–Science and Technology*, Vol. 18, No. 1, 2006, p. 31. https://doi.org/10.1007/BF02908417

[58] Marchetta, J., and Winter, A., "Simulation of Magnetic Positive Positioning for Space Based Fluid Management Systems," *Mathematical and Computer Modelling*, Vol. 51, No. 9, 2010, pp. 1202–1212. https://doi.org/10.1016/j.mcm.2010.01.002

[59] Romero-Calvo, A., Maggi, F., and Schaub, H., "Magnetic Positive Positioning: Toward the Application in Space Propulsion," *Acta Astronautica*, Vol. 187, 2021, pp. 348–361. https://doi.org/10.1016/j.actaastro.2021.06.045

[60] Romero-Calvo, A., Cano Gómez, G., Castro-Hernández, E., and Maggi, F., "Free and Forced Oscillations of Magnetic Liquids Under Low-Gravity Conditions," *Journal of Applied Mechanics*, Vol. 87, No. 2, 2019, Paper 021010.

[61] Romero-Calvo, A., García-Salcedo, A. J., Garrone, F., Rivoalen, I., Cano-Gómez, G., Castro-Hernández, E., Gutiérrez, M. A. H., and Maggi, F., "StELIUM: A Student Experiment to Investigate the Sloshing of Magnetic Liquids in Microgravity," *Acta Astronautica*, Vol. 173, Aug. 2020, pp. 344–355. https://doi.org/10.1016/j.actaastro.2020.04.013

[62] Koza, J. A., Mühlenhoff, S., Żabiński, P., Nikrityuk, P. A., Eckert, K., Uhlemann, M., Gebert, A., Weier, T., Schultz, L., and Odenbach, S., "Hydrogen Evolution Under the Influence of a Magnetic Field," *Electrochimica Acta*, Vol. 56, No. 6, 2011, pp. 2665–2675. https://doi.org/10.1016/j.electacta.2010.12.031

[63] Wang, M., Wang, Z., Gong, X., and Guo, Z., "The Intensification Technologies to Water Electrolysis for Hydrogen Production–A Review," *Renewable and Sustainable Energy Reviews*, Vol. 29, Jan. 2014, pp. 573–588. https://doi.org/10.1016/j.rser.2013.08.090

[64] Lin, M.-Y., Hourng, L.-W., and Kuo, C.-W., "The Effect of Magnetic Force on Hydrogen Production Efficiency in Water Electrolysis," *International Journal of Hydrogen Energy*, Vol. 37, No. 2, 2012, pp. 1311–1320. https://doi.org/10.1016/j.ijhydene.2011.10.024

[65] Lin, M. Y., and Hourng, L. W., "Effects of Magnetic Field and Pulse Potential on Hydrogen Production via Water Electrolysis," *International Journal of Energy Research*, Vol. 38, No. 1, 2014, pp. 106–116. https://doi.org/10.1002/er.3112

[66] Lin, M. Y., Hourng, L. W., and Hsu, J. S., "The Effects of Magnetic Field on the Hydrogen Production by Multielectrode Water Electrolysis," *Energy Sources, Part A: Recovery, Utilization, and Environmental Effects*, Vol. 39, No. 3, 2017, pp. 352–357. https://doi.org/10.1080/15567036.2016.1217289

[67] Kaya, M. F., Demir, N., Albawabiji, M. S., and Taş, M., "Investigation of Alkaline Water Electrolysis Performance for Different Cost Effective Electrodes Under Magnetic Field," *International Journal of Hydrogen Energy*, Vol. 42, No. 28, 2017, pp. 17,583–17,592. https://doi.org/10.1016/j.ijhydene.2017.02.039

[68] Bidin, N., Azni, S. R., Islam, S., Abdullah, M., Ahmad, M. F. S., Krishnan, G., Johari, A. R., Bakar, M. A. A., Sahidan, N. S., Musa, N., Salebi, M. F., Razali, N., and Sanagi, M. M., "The Effect of Magnetic and Optic Field in Water Electrolysis," *International Journal of Hydrogen Energy*, Vol. 42, No. 26, 2017, pp. 16,325–16,332. https://doi.org/10.1016/j.ijhydene.2017.05.169

[69] Garcés-Pineda, F. A., Blasco-Ahicart, M., Nieto-Castro, D., López, N., and Galán-Mascarós, J. R., "Direct Magnetic Enhancement of Electrocatalytic Water Oxidation in Alkaline Media," *Nature Energy*, Vol. 4, No. 6, 2019, pp. 519–525. https://doi.org/10.1038/s41560-019-0404-4

[70] Liu, Y., Pan, L. M., Liu, H., Chen, T., Yin, S., and Liu, M., "Effects of Magnetic Field on Water Electrolysis Using Foam Electrodes," *International Journal of Hydrogen Energy*, Vol. 44, No. 3, 2019, pp. 1352–1358. https://doi.org/10.1016/j.ijhydene.2018.11.103

[71] Liu, H., Xu, H., Pan, L. M., Zhong, D. H., and Liu, Y., "Porous Electrode Improving Energy Efficiency Under Electrode-Normal Magnetic Field in Water Electrolysis," *International Journal of Hydrogen Energy*, Vol. 44, No. 41, 2019, pp. 22,780–22,786. https://doi.org/10.1016/j.ijhydene.2019.07.024

[72] Hamidi, N., Sasongko, M. N., Widhiyanuriyawan, D., and Wardana, I., "Strengthening External Magnetic Fields with Activated Carbon Graphene for Increasing Hydrogen Production in Water Electrolysis," *International Journal of Hydrogen Energy*, Vol. 45, No. 38, 2020, pp. 19,370–19,380. https://doi.org/10.1016/j.ijhydene.2020.05.148

[73] Kamel, M. S., and Lezsovits, F., "Enhancement of Pool Boiling Heat Transfer Performance Using Dilute Cerium Oxide/Water Nanofluid: An Experimental Investigation," *International Communications in Heat and Mass Transfer*, Vol. 114, May 2020, Paper 104587. https://doi.org/10.1016/j.icheatmasstransfer.2020.104587

[74] Vatani, A., Woodfield, P. L., Dinh, T., Phan, H.-P., Nguyen, N.-T., and Dao, D. V., "Degraded Boiling Heat Transfer from Hotwire in Ferrofluid Due to Particle Deposition," *Applied Thermal Engineering*, Vol. 142, Sept. 2018, pp. 255–261. https://doi.org/10.1016/j.applthermaleng.2018.06.064

[75] Rosensweig, R. E., "Stress Boundary-Conditions in Ferrohydrodynamics," *Industrial & Engineering Chemistry Research*, Vol. 46, No. 19, 2007, pp. 6113–6117. https://doi.org/10.1021/ie060657e

[76] Engel, A., and Friedrichs, R., "On the Electromagnetic Force on a Polarizable Body," *American Journal of Physics*, Vol. 70, No. 4, 2002, pp. 428–432. https://doi.org/10.1119/1.1432971.

[77] Rosensweig, R. E., "Continuum Equations for Magnetic and Dielectric Fluids with Internal Rotations," *Journal of Chemical Physics*, Vol. 121, No. 3, 2004, pp. 1228–1242. https://doi.org/10.1063/1.1755660

[78] Rosensweig, R. E., *Ferrohydrodynamics*, Dover Publ. Inc., Mineola, NY, 1997, Chaps. V, VIII.

[79] Romero-Calvo, A., Cano-Gómez, G., Hermans, T. H., Benítez, L. P., Gutiérrez, M. A. H., and Castro-Hernández, E., "Total Magnetic Force on a Ferrofluid Droplet in Microgravity," *Experimental Thermal and Fluid Science*, Vol. 117, Sept. 2020, Paper 110124. https://doi.org/10.1016/j.expthermflusci.2020.110124

[80] Kuchel, P., Chapman, B., Bubb, W., Hansen, P., Durrant, C., and Hertzberg, M., "Magnetic Susceptibility: Solutions, Emulsions, and Cells," *Concepts in Magnetic Resonance Part A*, Vol. 18A, No. 1, 2003, pp. 56–71. https://doi.org/10.1002/cmr.a.10066

[81] Pickering, W. F., *Modern Analytical Chemistry*, Dekker, New York, 1971, Chap. 7, Sec. II.

[82] Bain, G. A., and Berry, J. F., "Diamagnetic Corrections and Pascal's Constants," *Journal of Chemical Education*, Vol. 85, No. 4, 2008, p. 532. https://doi.org/10.1021/ed085p532

[83] Lide, D. R., *CRC Handbook of Chemistry and Physics: 84th Edition*, CRC Press, Boca Ratón, FL, 2003, Sec. 8.

[84] Angulo, A., van der Linde, P., Gardeniers, H., Modestino, M., and Rivas, D. F., "Influence of Bubbles on the Energy Conversion Efficiency of Electrochemical Reactors," *Joule*, Vol. 4, No. 3, 2020, pp. 555–579. https://doi.org/10.1016/j.joule.2020.01.005

[85] Duhar, G., and Colin, C., "Dynamics of Bubble Growth and Detachment in a Viscous Shear Flow," *Physics of Fluids*, Vol. 18, No. 7, 2006, Paper 077101. https://doi.org/10.1063/1.2213638

[86] Stephan, K., *Physical Fundamentals of Vapor Bubble Formation*, Springer, Berlin, 1992, pp. 126–139. https://doi.org/10.1007/978-3-642-52457-8_10

[87] Vogt, H., and Balzer, R., "The Bubble Coverage of Gas-Evolving Electrodes in Stagnant Electrolytes," *Electrochimica Acta*, Vol. 50, No. 10, 2005, pp. 2073–2079. https://doi.org/10.1016/j.electacta.2004.09.025

[88] Landau, L., and Lifshitz, E., "Chapter I–Ideal Fluids," *Fluid Mechanics (Second Edition)*, edited by L. Landau, and E. Lifshitz, 2nd ed., Pergamon Press, Oxford, England, U.K., 1987, pp. 30–31. https://doi.org/10.1016/B978-0-08-033933-7.50009-X

[89] Kohonen, M. M., Karaman, M. E., and Pashley, R. M., "Debye Length in Multivalent Electrolyte Solutions," *Langmuir*, Vol. 16, No. 13, 2000, pp. 5749–5753. https://doi.org/10.1021/la991621c

[90] Sarwar, A., Nemirovski, A., and Shapiro, B., "Optimal Halbach Permanent Magnet Designs for Maximally Pulling and Pushing Nanoparticles," *Journal of Magnetism and Magnetic Materials*, Vol. 324, No. 5, 2012, pp. 742–754. https://doi.org/10.1016/j.jmmm.2011.09.008

[91] Shapiro, B., Kulkarni, S., Nacev, A., Sarwar, A., Preciado, D., and Depireux, D., "Shaping Magnetic Fields to Direct Therapy to Ears and Eyes," *Annual Review of Biomedical Engineering*, Vol. 16, No. 1, 2014, pp. 455–481. https://doi.org/10.1146/annurev-bioeng-071813-105206

[92] Barnsley, L. C., Carugo, D., Owen, J., and Stride, E., "Halbach Arrays Consisting of Cubic Elements Optimised for High Field Gradients in Magnetic Drug Targeting Applications," *Physics in Medicine and Biology*, Vol. 60, No. 21, 2015, pp. 8303–8327. https://doi.org/10.1088/0031-9155/60/21/8303

[93] Subramanian, M., Miaskowski, A., Jenkins, S. I., Lim, J., and Dobson, J., "Remote Manipulation of Magnetic Nanoparticles Using Magnetic Field Gradient to Promote Cancer Cell Death," *Applied Physics A*, Vol. 125, No. 4, 2019, p. 226. https://doi.org/10.1007/s00339-019-2510-3

[94] Bashyam, A., Li, M., and Cima, M. J., "Design and Experimental Validation of Unilateral Linear Halbach Magnet Arrays for Single-Sided Magnetic Resonance," *Journal of Magnetic Resonance*, Vol. 292, July 2018, pp. 36–43. https://doi.org/10.1016/j.jmr.2018.05.004

[95] Cooley, C. Z., Haskell, M. W., Cauley, S. F., Sappo, C., Lapierre, C. D., Ha, C. G., Stockmann, J. P., and Wald, L. L., "Design of Sparse Halbach Magnet Arrays for Portable MRI Using a Genetic Algorithm," *IEEE Transactions on Magnetics*, Vol. 54, No. 1, 2018, Paper 5100112. https://doi.org/10.1109/TMAG.2017.2751001

[96] Halbach, K., "Design of Permanent Multipole Magnets with Oriented Rare Earth Cobalt Material," *Nuclear Instruments and Methods*,

Vol. 169, No. 1, 1980, pp. 1–10.
https://doi.org/10.1016/0029-554X(80)90094-4

[97] Jackson, J. D., *Classical Electrodynamics*, 3rd ed., Wiley, New York, 1999, Chap. 2, Sec. 2.11.

[98] Liu, H., Pan, L. M., Huang, H., Qin, Q., Li, P., and Wen, J., "Hydrogen Bubble Growth at Micro-Electrode Under Magnetic Field," *Journal of Electroanalytical Chemistry*, Vol. 754, Oct. 2015, pp. 22–29.
https://doi.org/10.1016/j.jelechem.2015.06.015

[99] Hu, Q., Liu, H. B., Liu, Z., Zhong, D., Han, J., and Pan, L. M., "A Pair of Adjacent Bubbles Evolution at Micro-Electrode Under Electrode-Normal Magnetic Field," *Journal of Electroanalytical Chemistry*, Vol. 880, Jan. 2021, Paper 114886.
https://doi.org/10.1016/j.jelechem.2020.114886

D. P. Thunnissen
Associate Editor